

Article

Thermal Convection in Vesta's Core from Experimentally-Based Conductive Heat Flow Estimates

Oluwasanmi A. Orole , Wenjun Yong  and Richard A. Secco * 

Department of Earth Sciences, University of Western Ontario, London, ON N6A 3K7, Canada

* Correspondence: secco@uwo.ca

Abstract: Electrical resistivity measurements of Fe-5 wt% Ni were made in situ under pressures of 2–5 GPa and temperatures up to 2000 K in a cubic-anvil press. The thermal conductivity was calculated from the measured electrical resistivity data using the Wiedemann–Franz law. Comparison of these data with previous studies on pure Fe and Fe-10 wt% Ni shows that a change in the Ni content within the range 0–10 wt% Ni has no significant effect on electrical resistivity of Fe alloys. Comparing the estimated adiabatic core heat flux of ~331 MW at the top of Vesta's core to the range of estimated heat flux through the CMB of 1.5–78 GW, we infer that the mechanism stirring Vesta's liquid outer core to generate its surface magnetic field tens of millions of years ago in its early history was thermal convection.

Keywords: electrical resistivity; asteroid 4-vesta; iron-nickel alloys; magnetic fields; experimental techniques; high pressure; high temperature; thermal convection



Citation: Orole, O.A.; Yong, W.; Secco, R.A. Thermal Convection in Vesta's Core from Experimentally-Based Conductive Heat Flow Estimates. *Crystals* **2022**, *12*, 1752. <https://doi.org/10.3390/cryst12121752>

Academic Editors: Simone Anzellini, Daniel Errandonea, Anna Herlihy and Robin Turnbull

Received: 9 November 2022

Accepted: 30 November 2022

Published: 3 December 2022

Publisher's Note: MDPI stays neutral with regard to jurisdictional claims in published maps and institutional affiliations.



Copyright: © 2022 by the authors. Licensee MDPI, Basel, Switzerland. This article is an open access article distributed under the terms and conditions of the Creative Commons Attribution (CC BY) license (<https://creativecommons.org/licenses/by/4.0/>).

1. Introduction

Most terrestrial planets possess a core composed of a solid inner core and a liquid outer core. Flow of liquid in the outer core results in the generation of an internal magnetic field on terrestrial bodies [1]. A major energy source of fluid motion is thermal convection which is active when thermal conduction, or outer core adiabatic heat flow, is insufficient to provide the heat required to traverse the core-mantle boundary (CMB). From models of core evolution for the best-studied planet, Earth, the evolutionary pathways of terrestrial bodies during cooling are directly influenced by the thermal conductivity of the Fe alloys comprising their cores. Results from previous experimental studies [2–17] indicate that thermal conductivity of Fe alloys is dependent on pressure (P) and temperature (T). In order to determine the adiabatic heat flow inside the liquid core of a terrestrial body, effects of P and T on thermal conductivity of core-mimetic alloys must be known. Comparing the determined adiabatic heat flow with a knowledge of the heat flow through the CMB, the likelihood of thermal convection can be assessed.

The results of the experiments carried out in this study are applied to understand the core dynamics of the asteroid 4-Vesta. As the second largest asteroid with a diameter of 525 km, Vesta is located in the main asteroid belt, is differentiated with a metallic core, and is thought to have emerged during the early formation of our solar system [18]. Although Vesta's core has been assumed to be composed of pure Fe [19], by comparing Howardite-Eucrite-Diogenite (HED) and chondritic meteorites [20], Vesta's core composition is estimated to contain ~92% Fe and ~8% Ni. HED meteorites are assumed to have been ejected from Vesta because they share similar properties such as comparative mineralogy and spectral reflectivity with Vesta [21,22].

Presently, Vesta does not possess a magnetic field but paleomagnetic studies performed on the meteorites from Vesta indicate that as far back as 3.69 billion years ago, the surface of Vesta had a magnetic field intensity of 2 μT from an internally generated magnetic field [23]. By comparison with other core-generated magnetic fields in terrestrial-type

planetary bodies, the generation of Vesta's past core dynamo is most likely a result of the motion of the liquid outer core caused by either compositional convection and/or thermal convection. Thermal convection could have stirred Vesta's liquid outer core at any time in the past, as long as heat transfer through the CMB from the liquid core exceeded the adiabatic heat flow in the core. The primary condition for compositional convection to help drive Vesta's dynamo is the presence of a solid Fe-rich inner core from which light alloying elements, dispelled into the fluid on inner core solidification, provide the buoyancy force for outward radial fluid movement [17].

The goal of this study is to assess whether thermal convection in Vesta's liquid outer core could have once powered its dynamo. The contribution of thermal convection to the total heat flow at the top of the liquid region of Vesta's core is estimated by comparing the conductive heat flux at the top of its core with the estimates of heat flow across its CMB. The conductive heat flux is derived from the thermal conductivity which is calculated from the experimentally measured electrical resistivity of Fe-5 wt% Ni in this study.

2. Methods

A wire-shaped sample of Fe-5 wt% Ni (custom purchase from chemPUR, 99.9% purity) was assembled into a cubic pressure cell and placed in a 1000-ton cubic anvil press. The sample was heated by passing a high alternating current of up to ~250 A through a cylindrical graphite furnace after the pressure had stabilized at the target value. As shown in Figure 1, the four-wire electrode method was used.

The electrodes were made of thermocouples of 95W5Re and 74W26Re wires (Type C thermocouple) so that in thermocouple mode, temperature measurements were made and in resistance mode, voltage drop measurement was made by propagating a constant current of 0.2 A, from a Keysight B2961A power source through two of the electrodes. A platinum (Pt) disc was used in the cell assembly to increase the contact between the sample and the thermocouple/electrodes and to delay the contamination of the thermocouple to ensure more accurate temperature readings.

A preheating run up to ~1023 K followed by quenching in each experiment guaranteed that all metal components of the experimental setup were in good contact. After the preheating run, resistivity measurements were made on heating from room temperature to the final run temperature. Temperature was then quenched by shutting off the power to the furnace. A current polarity switch was used to eliminate any parasitic potentials and to obtain several voltage readings for both negative and positive currents at a given temperature. The resistivity of Fe-5 wt% Ni as a function of temperature and pressure was determined from averaging ~10 voltage readings taken by a Keysight 34470A data acquisition meter operating at 20 Hz, into a single data point per temperature value. Ohm's and Pouillet's laws were used to propagate the observed voltage error value (standard deviation of the voltage measurements) using the standard of formalism of Bevington and Robinson [24].

By measuring the electrical resistivity of Fe-5 wt% Ni at pressures of 2–5 GPa and temperatures into the liquid state, thermal conductivity of Fe-5 wt% Ni was calculated from electrical resistivity using the Wiedemann Franz law, $\kappa = LT/\rho$ [25] where ρ is the electrical resistivity at a specific P and T, L is the Lorenz number (with a theoretically calculated Sommerfeld value, L_0 , of $2.445 \times 10^{-8} \text{ W}\Omega\text{K}^{-2}$) and κ is thermal conductivity. The recovered pressure cell assembly after each experimental run was dismantled to retrieve the boron nitride sleeve housing the sample. A Nikon SMZ800 microscope was used to take photographs of each polishing stage of the sample as shown in Figure 2a and the value for the length and diameter of the sample at each polishing stage were recorded on the cross-section photographs as shown in Figure 2b.

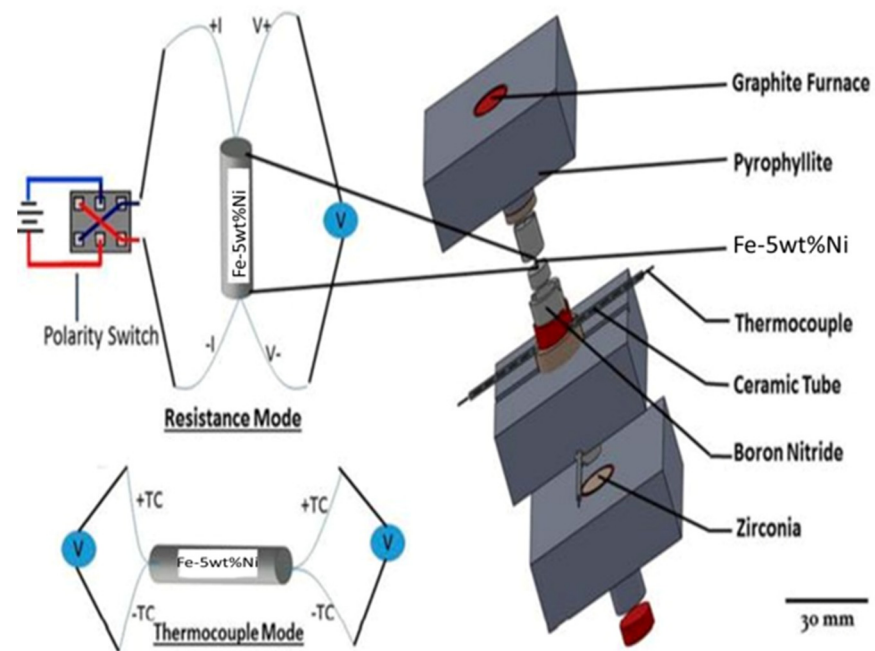


Figure 1. Schematic diagram of cell design (modified from Ezenwa and Secco [26]).

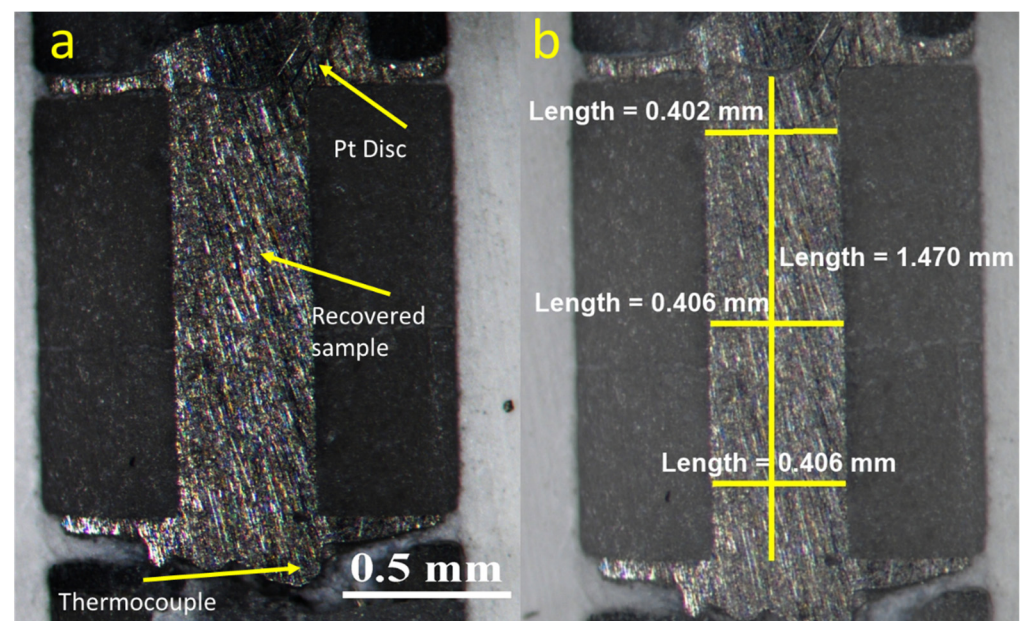


Figure 2. Cross sectional image of Fe-5 wt% Ni recovered from 4 GPa and 1986 K (a) Cross sectional image of a polishing stage of the sample (b) Cross sectional image of a polishing stage of the sample with the value for the length and diameter recorded.

After reaching the center of the sample, the polished cross-section was encased in epoxy prior to electron microprobe analysis (EMPA) of chemical composition using a JEOL JXA-8530F field-emission electron microprobe manufactured by JEOL Ltd in Tokyo, Japan with a 50 nA probe current, 20 kV accelerating voltage, and 10 μm spot-size beam.

3. Results

Post-experimental analysis indicated that the sample retained its cylindrical geometry and was well-contained even at temperatures into the liquid state, as shown in Figure 2. Progressive contamination of Pt from the disc into the sample occurs at higher temperatures

above the melting temperature. The highest temperature experimental runs were heated to ~ 270 K above melting and at these high temperatures, there is significant contamination from Pt. To understand at what temperature Pt contamination in the sample started, tests were conducted in two separate runs at 4 GPa at the following temperature conditions: 55 K below melting temperature followed by quenching, 54 K above melting temperature followed by quenching.

Both samples were recovered, analyzed and compared with the EMPA analysis of the 4 GPa resistivity run that was heated to 193 K above the melting temperature as shown in Figure 3a–c. The compositions for the recovered sample quenched at 55 K below the melting temperature (Figure 3a) shows that there is no contamination for temperature up to the melting temperature. The recovered sample that was quenched at 54 K above the melting temperature (Figure 3b) shows that contamination starts after melting and the amount of contamination is dependent on temperature, and thus time duration in the liquid state as shown in Figure 3b,c. Our calculation of thermal conductivity, from which core adiabatic heat flow is derived, relies on the resistivity value at the melting temperature. On the basis of these contamination test runs, this ensures that the sample is uncontaminated in the solid state and early liquid state and the resistivity values used represent values for Fe-5 wt% Ni.

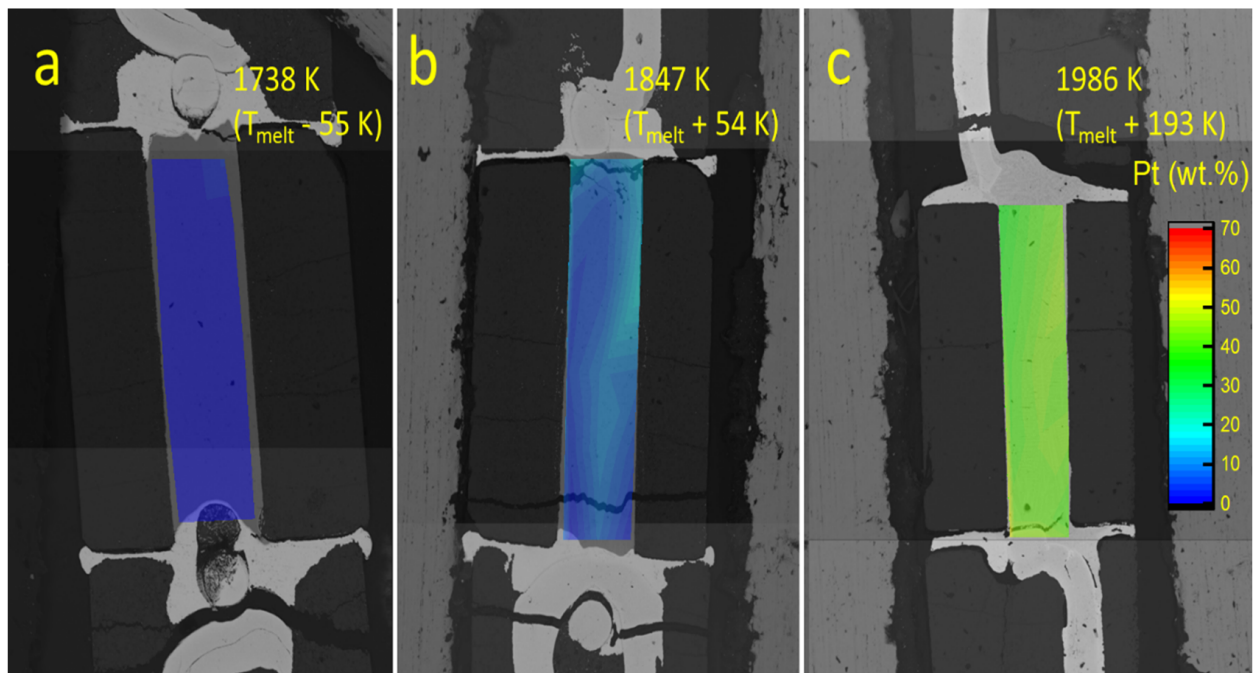


Figure 3. Chemical composition of Fe-5 wt% Ni recovered from three separate experiments at 4 GPa that reached maximum T of: (a) 1738 K ($T_{\text{melt}} - 55$ K); (b) 1847 K ($T_{\text{melt}} + 54$ K); and (c) 1986 K ($T_{\text{melt}} + 193$ K).

Figure 4 shows the electrical resistivity of Fe-5 wt% Ni as a function of temperature at pressures of 2–5 GPa. The magnetic transition at ~ 900 K and the melting at ~ 1800 K are visible on the plot. The noticeable similarities in the trends of the 2, 3, 4 and 5 GPa data indicate internal consistency and reproducibility. The thermal conductivity of Fe-5 wt% Ni was calculated using the Wiedemann Franz law. Although the Lorenz number may vary with pressure and temperature, this study uses the Sommerfeld value as a representative value of the Lorenz number [12] to calculate the thermal conductivity of Fe-5 wt% Ni since we are not aware of a specific Lorenz value for Fe-5 wt% Ni. The thermal conductivity plot, given in Figure 5, shows a sudden increase at the magnetic transition (~ 900 K) of Fe-5 wt% Ni and a decrease of thermal conductivity on melting.

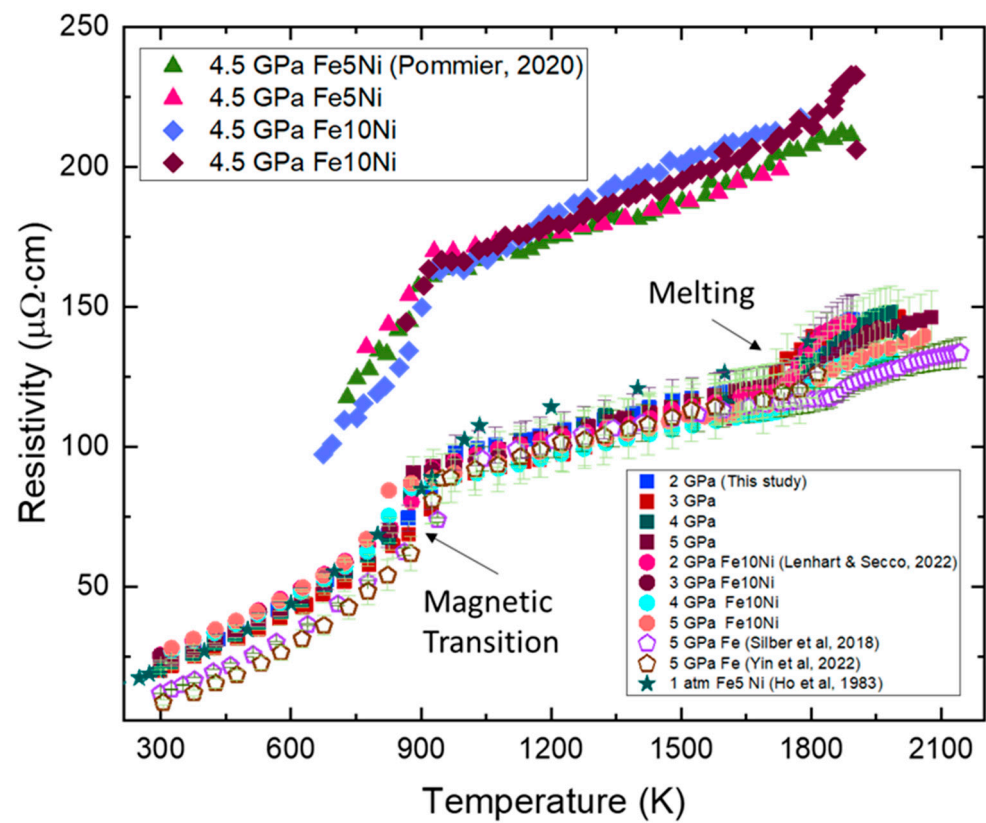


Figure 4. Comparison of the electrical resistivity of Fe-5 wt% Ni and Fe-10 wt% Ni [11,17,27–29].

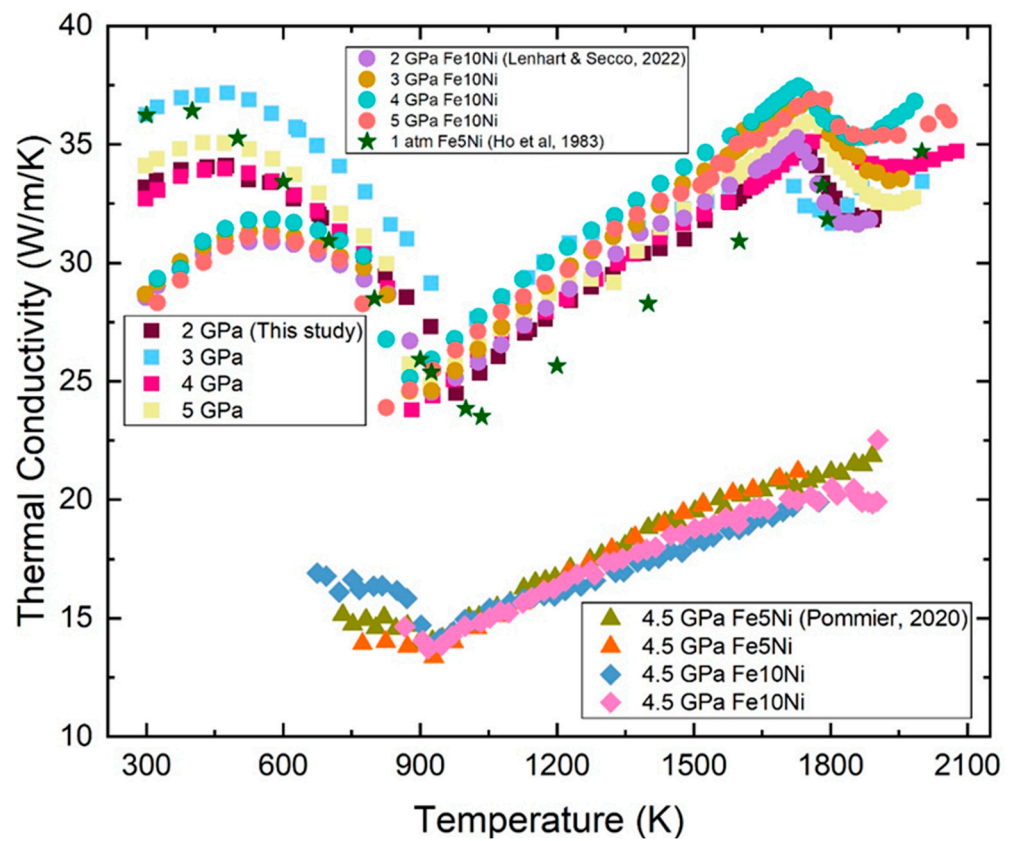


Figure 5. Comparison of thermal conductivity of Fe-5 wt% Ni and Fe-10 wt% Ni [17,27,28].

4. Discussion

From Figures 4 and 5, there are noticeable similarities in the trends of the results for this study and those of previous studies [17,27,28] with similar sample composition. The expected trend of decreasing resistivity with increasing pressure can be seen in the high temperature region when comparing the data from this study to the 1 atm data from Ho et al. [17]. The dataset by Pommier [28] shows the opposite trend. Comparison of the electrical resistivity and thermal conductivity data (Figures 4 and 5) of Fe-5 wt% Ni from this study with Fe-10 wt% Ni from Lenhart and Secco [27], and separate comparison of the Fe-5 wt% Ni with Fe-10 wt% Ni from Pommier [28] indicates that the change in the Ni content of up to 10 wt% has no significant effect on the electrical resistivity and thermal conductivity values of Fe-Ni alloys.

Figure 6 shows measured electrical resistivity and calculated thermal conductivity data at 1800 K and high pressures from this study plotted with 1 atm data [17] at 1800 K for the purpose of interpolation to Vestan CMB pressure of 0.2 GPa. At 1 atm, the resistivity datum was measured [17] and thermal conductivity was calculated in the same way as for the high-pressure data. The ideal Lorenz number (L_0) was used in the calculations for this study because the exact value for the Lorenz number for Fe-5 wt% Ni is unknown. Since our composition is 95 wt% Fe, our use of L_0 is consistent with the calculated values of L/L_0 that show a variation of 1.01–1.06 along the melting boundary of pure Fe in the pressure range 2–5 GPa [14]. This approach is also consistent with the conclusions of another study that states that the Sommerfeld value is a good approximation for terrestrial cores [4]. The trend lines shown in Figure 6 between the ambient pressure data from Ho et al. [17] and this study (2–5 GPa) supports the interpolation of electrical resistivity and thermal conductivity at pressure values in Vesta's core. The estimated pressure at Vesta's center (0.2–0.3 GPa) is approximately double the pressure at Vesta's CMB (0.1–0.2 GPa) [18]. The adiabatic heat flux at the top of Vesta's core is estimated by using the thermal conductivity value of Fe-5 wt% Ni at each pressure just after melting: (2 GPa, 32.6 W/m/K), (3 GPa, 33.7 W/m/K), (4 GPa, 33.2 W/m/K), (5 GPa, 33.4 W/m/K) and the thermal conductivity value for Fe-5 wt% Ni at ambient pressure just after melting [17] to interpolate to 0.2 GPa the thermal conductivity value of Fe-5 wt% Ni ($\kappa = 34.1$ W/m/K).

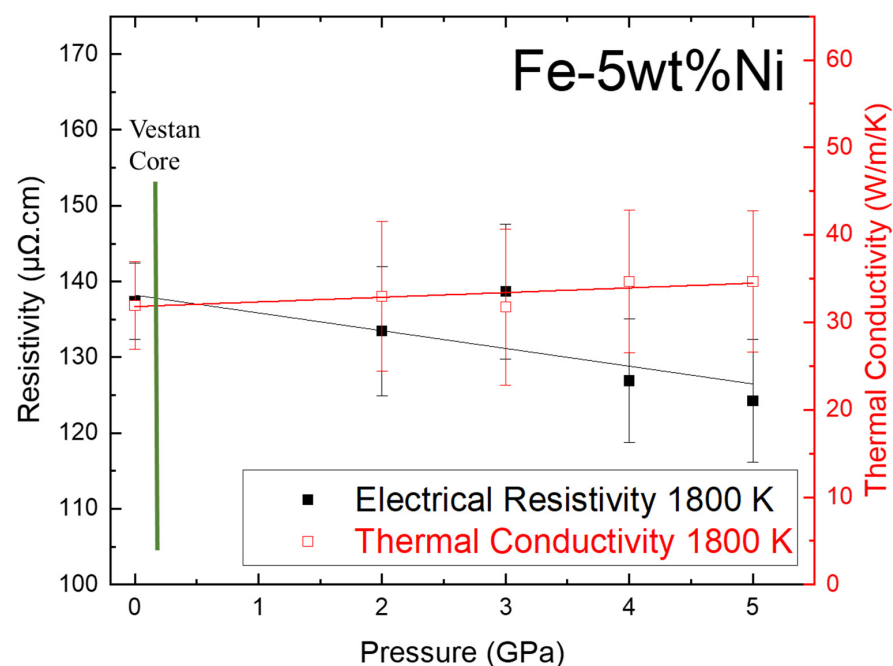


Figure 6. High pressure electrical resistivity and thermal conductivity data at 1800 K from this study plotted with 1 atm data [17] for purpose of interpolation to Vestan CMB pressure of 0.2 GPa.

The adiabatic heat flux density (~ 2.2 mW/m²) was calculated using Fourier's law for heat transfer $q = -\kappa \nabla T$, where $\kappa = 34.1$ W/m/K and the temperature gradient in the core, $\nabla T = -0.06$ K/km from the equation $\nabla T = -\alpha g T / C_p$ when α (thermal expansion coefficient) is 10^{-4} K⁻¹, g (gravitational acceleration) is 0.3 m/s², T is 1700 K and C_p (isobaric heat capacity) is 800 J kg⁻¹ K⁻¹ [27].

Using the equation $Q_{ad} = -4\pi r^2 \kappa \nabla T$ and radius $r = 110$ km (under the assumption of radial symmetry), the total adiabatic heat flux at the top of Vesta's core is ~ 331 MW. The estimated adiabatic heat flux density of ~ 2.2 mW/m² and the heat flow of ~ 331 MW at the top of Vesta's early core in this study are much smaller than the estimated heat flux density of 10 – 500 mW/m² and the corresponding heat flow of ~ 1.5 – 78 GW through Vesta's early CMB [17,30]. Since the calculated adiabatic heat flow is very much smaller than the heat flow through the CMB, thermal convection is necessary to transport heat within the core to the CMB. This indicates the strong likelihood that the mechanism stirring Vesta's liquid outer core to generate its surface magnetic field for tens of millions of years in its early history was thermal convection.

The estimated values of adiabatic heat flow in the core from this study are based on thermal conductivity values calculated from our electrical resistivity measurements while the estimated heat flow values through Vesta's early CMB are from modelling in previous studies. The accuracy of these two approaches is dependent on other parameters like the temperature gradient inside Vesta, and some of these parameters are not well constrained.

Apart from Ni in Vesta's core, some authors propose [31,32] the presence of other light elements like S and Si. Although the range of increase to the electrical resistivity is uncertain, S increases the electrical resistivity of the Fe alloy melt at high pressures [5,13]. The presence of S infers a lower density estimate for an Fe-S core which increases the estimated characteristic length because a higher core radius will be derived from the gravitational study of Russell et al. [22]. The presence of small amount of Si does not change the electrical resistivity of liquid Fe as indicated by the study done by Silber et al. [10] on Fe-4.5 wt% Si which shows that the electrical resistivity of liquid Fe alloys is constant along the melting curve and also similar to the electrical resistivity of pure Fe.

5. Conclusions

Comparing the result of this study with those of pure Fe and Fe-10 wt% Ni [12,17,27,28] at similar pressures shows that at high temperatures, Ni contents of up to 10 wt% in pure liquid Fe does not significantly increase the electrical resistivity. Therefore, thermal convection is the most likely energy source mechanism for Vesta's past core dynamo because the estimated adiabatic heat flux density of ~ 2.2 mW/m² at the top of Vesta's early core is much smaller than the heat flux density estimates across Vesta's early CMB.

Author Contributions: Conceptualization, R.A.S.; methodology, O.A.O. and W.Y.; validation, W.Y. and R.A.S.; formal analysis, O.A.O.; investigation, O.A.O. and W.Y.; resources, R.A.S. and W.Y.; data curation, O.A.O.; writing—original draft preparation, O.A.O.; writing—review and editing, W.Y. and R.A.S.; supervision, W.Y. and R.A.S.; project administration, R.A.S.; funding acquisition, R.A.S. and W.Y. All authors have read and agreed to the published version of the manuscript.

Funding: This research was funded by the Natural Sciences and Engineering Research Council of Canada, grant number RGPIN 2018-05021 to R.A.S., grant numbers RGPIN-2022-04427 and DGECR-2022-00151 to W.Y.

Data Availability Statement: The data presented in this study is openly available at <https://data.mendeley.com/datasets/8sk8fk3hmb/1> (8 November 2022).

Acknowledgments: We thank Jonathan Jacobs for his help with machining of experimental components. We thank the three anonymous reviewers for their constructive comments that improved this manuscript.

Conflicts of Interest: The authors declare no conflict of interest. The funders had no role in the design of the study; in the collection, analyses, or interpretation of data; in the writing of the manuscript, or in the decision to publish the results.

References

1. Roberts, P.H. On the Thermal Instability of a Rotating-Fluid Sphere Containing Sources. *Philos. Tran. R. Soc. Lond. A* **1968**, *263*, 93–117.
2. Berrada, M.; Secco, R.A.; Yong, W. Resistivity of Solid and Liquid Fe–Ni–Si with Applications to the Cores of Earth, Mercury and Venus. *Sci. Rep.* **2022**, *12*, 9941. [[CrossRef](#)] [[PubMed](#)]
3. Berrada, M.; Secco, R.A.; Yong, W. Adiabatic Heat Flow in Mercury’s Core from Electrical Resistivity Measurements of Liquid Fe–8.5 wt%Si to 24 GPa. *Earth Planet. Sci. Lett.* **2021**, *568*, 117053. [[CrossRef](#)]
4. Gomi, H.; Hirose, K. Electrical Resistivity and Thermal Conductivity of Hcp Fe–Ni Alloys under High Pressure: Implications for Thermal Convection in the Earth’s Core. *Phys. Earth Planet. Inter.* **2015**, *247*, 2–10. [[CrossRef](#)]
5. Littleton, J.A.H.; Secco, R.A.; Yong, W. Thermal Convection in the Core of Ganymede Inferred from Liquid Eutectic Fe–FeS Electrical Resistivity at High Pressures. *Crystals* **2021**, *11*, 875. [[CrossRef](#)]
6. Littleton, J.A.H.; Secco, R.A.; Yong, W. Electrical Resistivity of FeS at High Pressures and Temperatures: Implications of Thermal Transport in the Core of Ganymede. *J. Geophys. Res. Planets* **2021**, *126*, e2020JE006793. [[CrossRef](#)]
7. Pommier, A.; Davies, C.J.; Zhang, R. A Joint Experimental-Modeling Investigation of the Effect of Light Elements on Dynamos in Small Planets and Moons. *J. Geophys. Res. Planets* **2020**, *125*, 006492. [[CrossRef](#)]
8. Berrada, M.; Secco, R.A.; Yong, W.; Littleton, J.A.H. Electrical Resistivity Measurements of Fe–Si with Implications for the Early Lunar Dynamo. *J. Geophys. Res. Planets* **2020**, *125*, e2020JE006380. [[CrossRef](#)]
9. Yong, W.; Secco, R.A.; Littleton, J.A.H.; Silber, R.E. The Iron Invariance: Implications for Thermal Convection in Earth’s Core. *Geophys. Res. Lett.* **2019**, *46*, 11065–11070. [[CrossRef](#)]
10. Silber, R.E.; Secco, R.A.; Yong, W.; Littleton, J.A.H. Heat Flow in Earth’s Core from Invariant Electrical Resistivity of Fe–Si on the Melting Boundary to 9 GPa. Do Light Elements Matter? *J. Geophys. Res. Solid Earth* **2019**, *124*, 5521–5543. [[CrossRef](#)]
11. Silber, R.E.; Secco, R.A.; Yong, W.; Littleton, J.A.H. Electrical Resistivity of Liquid Fe to 12 GPa: Implications for Heat Flow in Cores of Terrestrial Bodies. *Sci. Rep.* **2018**, *8*, 10758. [[CrossRef](#)]
12. Zhang, Y.; Hou, M.; Driscoll, P.; Salke, N.P.; Liu, J.; Greenberg, E.; Prakapenka, V.B.; Lin, J.-F. Transport Properties of Fe–Ni–Si Alloys at Earth’s Core Conditions: Insight into the Viability of Thermal and Compositional Convection. *Earth Planet. Sci. Lett.* **2021**, *553*, 116614. [[CrossRef](#)]
13. Pommier, A. Influence of Sulfur on the Electrical Resistivity of a Crystallizing Core in Small Terrestrial Bodies. *Earth Planet. Sci. Lett.* **2017**, *496*, 37–46. [[CrossRef](#)]
14. Secco, R.A. Thermal Conductivity and Seebeck Coefficient of Fe and Fe–Si Alloys: Implications for Variable Lorenz Number. *Phys. Earth Planet. Inter.* **2017**, *265*, 23–34. [[CrossRef](#)]
15. Ezenwa, I.C.; Secco, R.A. Constant Electrical Resistivity of Zn along the Melting Boundary up to 5 GPa. *High Press. Res.* **2017**, *37*, 319–333. [[CrossRef](#)]
16. Gomi, H.; Hirose, K.; Akai, H.; Fei, Y. Electrical Resistivity of Substitutionally Disordered Hcp Fe–Si and Fe–Ni Alloys: Chemically-Induced Resistivity Saturation in the Earth’s Core. *Earth Planet. Sci. Lett.* **2016**, *451*, 51–61. [[CrossRef](#)]
17. Ho, C.Y.; Ackerman, M.W.; Wu, K.Y.; Havill, T.N.; Bogaard, R.H.; Matula, R.A.; Oh, S.G.; James, H.M. Electrical Resistivity of Ten Selected Binary Alloy Systems. *J. Phys. Chem. Ref. Data* **1983**, *12*, 183–322. [[CrossRef](#)]
18. McSween, H.Y.; Huss, G.R. *Cosmo Chemistry*; Cambridge University Press: Cambridge, UK, 2010.
19. Formisano, M.; Federico, C.; Angelis, S.; Sanctis, M.C.; Magni, G. A core dynamo in Vesta? *Mon. Not. R. Astron. Soc. Lett.* **2016**, *458*, 695–707. [[CrossRef](#)]
20. Dreibus, G.; Bruckner, J.; Wanke, H. On the Core Mass of the Asteroid Vesta. *Meteorite. Planet. Sci.* **1997**, *32*, 36.
21. McCord, T.B.; Adams, J.B.; Johnson, T.V. Asteroid Vesta: Spectral Reflectivity and Compositional Implications. *Science* **1970**, *168*, 1445–1447. [[CrossRef](#)] [[PubMed](#)]
22. Russell, C.T.; Raymond, C.A.; Coradini, A.; McSween, H.Y.; Zuber, M.T.; Nathues, A.; Sanctis, M.C.; Jaumann, R.; Konopliv, A.S.; Preusker, F.; et al. Dawn at Vesta: Testing the Protoplanetary Paradigm. *Science* **2012**, *336*, 684–686. [[CrossRef](#)]
23. Fu, R.R.; Weiss, B.P.; Shuster, D.L.; Gattacceca, J.; Grove, T.L.; Suavet, C.; Lima, E.A.; Li, L.; Kuan, A.T. An Ancient Core Dynamo in Asteroid Vesta. *Science* **2012**, *338*, 238–241. [[CrossRef](#)]
24. Bevington, P.R.; Robinson, D.K. *Data Reduction and Error Analysis*; McGraw-Hill: New York, NY, USA, 2003.
25. Wiedemann, D.; Franz, R. Über die Wärme-Leitungsfähigkeit der Metalle. *Ann. Phys.* **1853**, *165*, 497–531.
26. Ezenwa, I.C.; Secco, R.A.; Yong, W.; Pozzo, M.; Alfè, D. Electrical Resistivity of Solid and Liquid Cu up to 5 GPa: Decrease along the Melting Boundary. *J. Phys. Chem. Solids* **2017**, *110*, 386–393. [[CrossRef](#)]
27. Lenhart, E.M.; Secco, R.A. Implications for the Energy Source for an Early Dynamo in Vesta from Experiments on Electrical Resistivity of Liquid Fe–10wt%Ni at High Pressures. *Icarus* **2022**, *378*, 114962. [[CrossRef](#)]
28. Pommier, A. Experimental Investigation of the Effect of Nickel on the Electrical Resistivity of Fe–Ni and Fe–Ni–S Alloys under Pressure. *Am. Mineral.* **2020**, *105*, 1069–1077. [[CrossRef](#)]
29. Yin, Y.; Wang, L.; Zhai, S.; Fei, Y. Electrical Resistivity of Fe and Fe–3 Wt%P at 5 GPa with Implications for the Moon’s Core Conductivity and Dynamo. *JGR Planets* **2022**, *127*, e2021JE007116. [[CrossRef](#)]
30. Weiss, B.P.; Gattacceca, J.; Stanley, S.; Rochette, P.; Christensen, U.R. Paleomagnetic Records of Meteorites and Early Planetary Differentiation. *Space Sci. Rev.* **2010**, *152*, 341–390. [[CrossRef](#)]

31. Zhang, A.-C.; Kawasaki, N.; Bao, H.; Liu, J.; Qin, L.; Kuroda, M.; Gao, J.-F.; Chen, L.-H.; He, Y.; Sakamoto, N.; et al. Evidence of Metasomatism in the Interior of Vesta. *Nat. Commun.* **2020**, *11*, 1289. [[CrossRef](#)] [[PubMed](#)]
32. Wu, N.; Farquhar, J.; Dottin, J.W.; Magalhães, N. Sulfur Isotope Signatures of Eucrites and Diogenites. *Geochim. Cosmochim. Acta* **2018**, *233*, 1–13. [[CrossRef](#)]